The Astronomical Journal, 146:139 (10pp), 2013 December doi:10.1088/0004-6256/146/6/139

PHOTOMETRY OF VARIABLE STARS FROM DOME A, ANTARCTICA: RESULTS FROM THE 2010 OBSERVING SEASON

Lingzhi Wang[1,2,3,13], Lucas M. Macri[2], Lifan Wang[2,3,4], Michael C. B. Ashley[5], Xiangqun Cui[3,6], Long-Long Feng[3,4], Xuefei Gong[3,6], Jon S. Lawrence[5,7], Qiang Liu[3,8], Daniel Luong-Van[5], Carl R. Pennypacker[9], Zhaohui Shang[3,10], John W. V. Storey[5], Huigen Yang[3,11], Ji Yang[3,4], Xiangyan Yuan[3,6], Donald G. York[12], Xu Zhou[3,8], Zhenxi Zhu[3,4], and Zonghong Zhu[1,3]

[1] Department of Astronomy, Beijing Normal University, Beijing 100875, China; wanglingzhi@bao.ac.cn
[2] Mitchell Institute for Fundamental Physics and Astronomy, Department of Physics and Astronomy, Texas A&M University, College Station, TX 77843, USA
[3] Chinese Center for Antarctic Astronomy, Nanjing 210008, China
[4] Purple Mountain Observatory, Chinese Academy of Sciences, Nanjing 210008, China
[5] School of Physics, University of New South Wales, NSW 2052, Australia
[6] Nanjing Institute of Astronomical Optics and Technology, Nanjing 210042, China
[7] Australian Astronomical Observatory, NSW 1710, Australia
[8] National Astronomical Observatory of China, Chinese Academy of Sciences, Beijing 100012, China
[9] Center for Astrophysics, Lawrence Berkeley National Laboratory, Berkeley, CA, USA
[10] Tianjin Normal University, Tianjin 300074, China
[11] Polar Research Institute of China, Pudong, Shanghai 200136, China
[12] Department of Astronomy and Astrophysics and Enrico Fermi Institute, University of Chicago, Chicago, IL 60637, USA
Received 2012 September 21; accepted 2013 September 12; published 2013 October 22

ABSTRACT

We present results from a season of observations with the Chinese Small Telescope ARray, obtained over 183 days of the 2010 Antarctic winter. We carried out high-cadence time-series aperture photometry of 9125 stars with $i \lesssim 15.3$ mag located in a 23 deg^2 region centered on the south celestial pole. We identified 188 variable stars, including 67 new objects relative to our 2008 observations, thanks to broader synoptic coverage, a deeper magnitude limit, and a larger field of view. We used the photometric data set to derive site statistics from Dome A. Based on two years of observations, we find that extinction due to clouds at this site is less than 0.1 and 0.4 mag during 45% and 75% of the dark time, respectively.

Key words: site testing – stars: variables: general

Online-only material: color figures, machine-readable and VO tables

1. INTRODUCTION

Synoptic (time-series) astronomy has undergone a dramatic transformation over the past decade thanks to advances in imaging and computer technology. Many high-impact discoveries have taken place, such as transiting exoplanets (Charbonneau et al. 2000) and the detection of supernovae mere hours after explosion (Nugent et al. 2011). These and other astrophysical problems benefit from long, continuous, and stable time-series photometry, which until recently could only be achieved from space or via coordinated observations by a world-wide telescope network. The former alternative is expensive, while the latter is fraught with calibration issues, variable weather across the sites, and is highly labor intensive.

One region on Earth—the Antarctic Plateau—offers an excellent alternative to the aforementioned options by providing a combination of extended periods of dark time, high altitude, low precipitable water vapor, extremely low temperatures and a very stable atmosphere with greatly reduced scintillation noise (Kenyon et al. 2006). These conditions enable new or extended observation windows in the infrared and sub-millimeter regions of the electromagnetic spectrum, as well as improved conditions at optical and other wavelengths. The resulting gains in sensitivity and photometric precision over the best temperate sites include factors of 20–100× lower sky background in the infrared and 3–4× lower scintillation noise at optical wavelengths (Storey 2005, 2007, 2009; see also Tables 2 and 4 and Figures 7–11 in Burton 2010). The long "winter night" that occurs at these latitudes and the minimal daily change in elevation for any given source make the performance of a polar site equivalent to that of a six-site network at temperate latitudes (Mosser & Aristidi 2007). Some disadvantages include the reduced fraction of the celestial sphere that can be observed, prolonged twilight, and possibility of aurorae.

According to meteorological studies carried out by Saunders et al. (2009, 2010), the region surrounding Dome A (elevation: 4,093 m above mean sea level) in the Antarctic plateau is likely the best astronomical site on Earth. In order to further investigate the conditions at this promising site, we developed an observatory capable of year-round operations called PLATO (Ashley et al. 2010; Luong-van et al. 2010; Yang et al. 2009; Lawrence et al. 2009; Lawrence et al. 2008; Hengst et al. 2008; Lawrence et al. 2006), and a quad-telescope called CSTAR (the Chinese Small Telescope ARray; Yuan et al. 2008; Zhou et al. 2010b). The observatory is part of the Chinese Kunlun station, located at Dome A.

Several papers were written based on a large amount of high-quality photometric data obtained during the 2008 Antarctic winter: Zou et al. (2010) undertook a variety of sky brightness, transparency, and photometric monitoring observations; Zhou et al. (2010a) published a photometric catalog of ∼10,000 stars; and Wang et al. (2011) presented the first catalog of variable stars in the CSTAR field of view.

This paper presents an analysis of the data acquired by the CSTAR#3 telescope during the 2010 Antarctic winter season. Section 2 briefly describes the observations and data reduction; Section 3 describes the steps followed to obtain high-precision

[13] Current address: National Astronomical Observatory of China, Chinese Academy of Sciences, Beijing 100012, China.

Table 1
Log of Observations

Month 2010	No. of Images	Total Exp. Time (hr)
Mar	1587	17.6
Apr	31,110	345.7
May	39,651	405.8
Jun	69,509	579.2
Jul	97,310	631.1
Aug	73,088	406.0
Sep	30,098	167.2
Total	342,353	2552.6

time-series photometry of the brightest 9125 stars with well-sampled light curves; Section 4 discusses the variable stars we discovered; and Section 5 contains our conclusions.

2. OBSERVATIONS AND DATA REDUCTION

2.1. Observations

Observations were carried out using the same CSTAR telescope (unit #3), which we described in detail in Wang et al. (2011). Briefly, it is a Schmidt–Cassegrain wide-field telescope with a pupil entrance aperture of 145 mm, a Sloan *i*-band filter, and a 1 K × 1 K frame-transfer CCD with a plate scale of $15\farcs7$ pixel^{-1}, giving a field of view $4\fdg5$ on a side. The telescope and camera have no moving parts, to allow for robust operation in the extreme conditions of the Antarctic winter. Therefore, the field of view is centered on the south celestial pole (SCP), which lies ∼9° from the zenith at this site, and exposures are short (20–40 s) to prevent star trails. The SCP field probes the inner halo of the Milky Way ($l = 303°, b = -27°$) and has moderate extinction ($A_i = 0.31$ mag; Schlafly & Finkbeiner 2011).

Scientifically useful images were acquired from 2010 March 29 to 2010 September 27. Table 1 lists the number of images and total integration time per month and Table 2 lists the different integration times used throughout the observing season. More than 338,000 images (equivalent to over 360 GB of data) were collected with a total integration time of 2553 hr.

2.2. Data Reduction

The preliminary data reduction for raw science frames involved bias subtraction, flat fielding, correction for variations in sky background, fringe pattern subtraction, and bad pixel masking. We used the same bias frame from our previous paper, which was created during instrument testing in China. We generated a sky flat by median-combining 2700 frames with high sky level (>10,000 ADU) taken throughout the observing season during twilight conditions (Sun elevation angle between 0° and −10°). Prior to combining the images, we masked any stars present in the individual frames using a detection threshold of 2σ, as well as regions within 10 pixels of any pixel close to saturation (defined as >25,000 ADU).

Approximately 35% of the bias-subtracted and flat-fielded images showed low-frequency sky background variations with an amplitude of ∼3% of the mean value, which we subtracted by the following method. We divided each image into 1024 square sections (32 pixels on a side) and computed the mean and standard deviation of the sky value in each section using the procedure implemented in DAOPHOT (Stetson 1987). We did not use any sections with sky values above 20,000 or below 0 ADU, or those with standard deviations that exceeded 300 ADU. Those properties are typical of very crowded regions of an image, or indicate the presence of a very bright star, so we replaced the sky value of those sections with the median value of their nearest ten neighbors. We generated a full-resolution background model frame by fitting the 1024 sky values using a thin-plate spline. We calculated the standard deviation of sky values before and after model subtraction; if the reduction in the scatter was less than a factor of two, we reduced the section size to 16 pixels on a side and repeated the procedure.

Table 2
Exposure Times

Start Date	End Date	Exp. (s)	No. of Images
2010 Mar 29	2010 May 26	40	59,843
2010 May 26	2010 Jul 13	30	114,577
2010 Jul 13	2010 Sep 27	20	167,933

The background-subtracted images exhibited a fringe pattern, which is commonly encountered in CCD images obtained at near-infrared wavelengths (for a review, see Howell 2012). We created a fringe correction frame and removed this instrumental signature from our images following these steps. First, we selected 1500 images taken each month with the lowest sky levels during dark time (Sun elevation angle below −18°) and 1500 images taken during twilight. This yielded seven sets of images obtained during twilight and five sets acquired during dark time (April to August). The motivation behind creating the two different sets was to check for variations in fringe amplitude as a function of Sun elevation angle.

Next, we removed stars by masking any pixel lying more than 2σ above the sky level. We combined the frames in each of the 12 sets by sorting the un-masked pixels at each (x, y) position, discarding the lowest 10 values (where the fringe pattern was too low to be useful), and averaging the next 50 values. The fringe pattern had an average peak-to-peak amplitude of 2% of the mean sky value, with no statistically significant variation as a function of time or Sun elevation angle. Therefore, we generated the final fringe frame by taking the minimum pixel value at each location among the 12 sets (to further ensure that no stellar sources were included). The fringe pattern was subtracted from individual frames by iteratively scaling the correction image until the sky background exhibited the lowest rms value.

3. PHOTOMETRY

3.1. Frame Selection and Photometry

We carried out initial photometric measurements on the debiased, flattened, sky-subtracted, and fringe-corrected images using the same pipeline and procedures described in Wang et al. (2011), which we briefly summarize here. Given the extremely undersampled nature of the images, we performed aperture photometry using DAOPHOT (Stetson 1987). We set the aperture radius to 2.5 pixels (equivalent to $39\farcs3$) and the sky annulus extended from 4 to 7 pixels (equivalent to $62\farcs8$–$109\farcs9$). The detection threshold was set to 5σ above the sky background, which typically corresponded to $i \sim 14$ mag.

Figure 1 displays the Sun elevation angle (top panel), sky background in ADU s^{-1} (middle panel), and number of stars detected (bottom panel) for each image as a function of time since 2010 March 29. The sky background shows a clear monthly pattern related to the lunar phase. During most of the

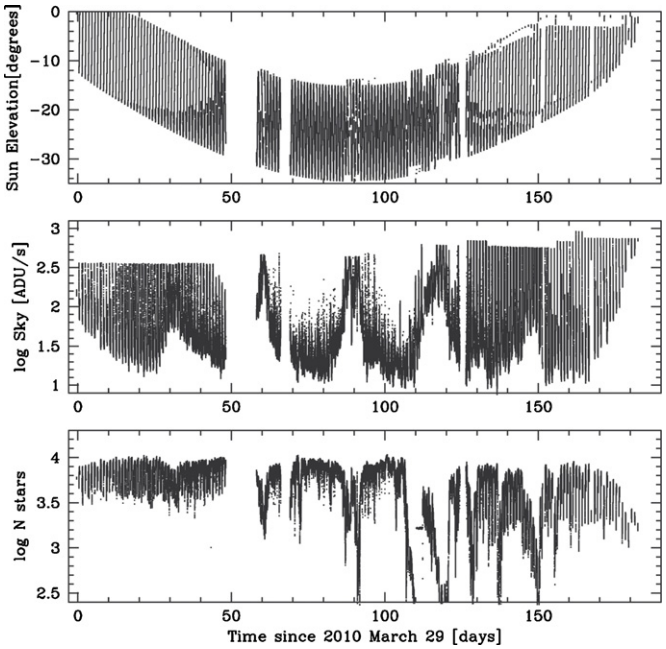

Figure 1. Time-series plots of the Sun elevation angle (top panel), sky brightness level (middle panel), and number of stars detected in each image (bottom panel).

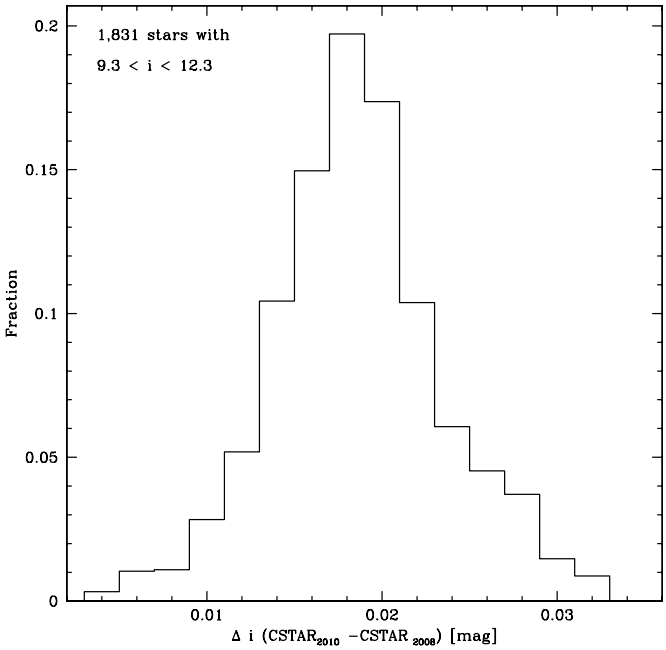

Figure 2. Comparison of the mean instrumental magnitudes of bright stars in common between the 2008 and 2010 CSTAR observations.

winter season, the data acquisition system was programmed to stop when the sky level exceeded 14,600 ADU; this limit was raised to 19,400 after 2010 September 7. We initially selected frames with Sun elevation angle below 0° and more than 1500 stars. These criteria were met by 85.5% (289,343) of all the images acquired during the Antarctic winter. A period of bad weather and ice buildup on the top cover of the instrument during the month of July resulted in the rejection of ∼35,000 images (equivalent to 8 days of operations).

The selected images have a median sky level of 32 ADU s^{-1}, equivalent to a median sky background of $i = 19.8$ mag arcsec^{-2}. This value is identical to the value derived by Zou et al. (2010) and similar to our previous determination of 19.6 mag arcsec^{-2} (Wang et al. 2011). Note that all these estimates include contributions from moonlight. The darkest sky background measured during the season (on clear moonless nights) was $i \sim 20.9$ mag arcsec^{-2}. The median value of the number of stars detected in an individual frame is 8600, higher than the corresponding value of 7500 from the 2008 observations. We attribute this increase to the subtraction of sky background variations described in Section 2.2, which enabled the detection of fainter stars at a fixed threshold.

We used the initial photometry to register all frames using DAOMATCH and DAOMASTER and created a reference image (hereafter "master frame") with 4× finer spatial sampling. We followed the same procedure described in our previous paper, this time based on 2580 high-quality images obtained during 2010 June 13. We carried out aperture photometry on the master frame using the same parameters listed above and detected approximately 155,000 stars, reaching a depth of $i \sim 20.9$ mag. Additionally, we performed point-spread function (PSF) photometry that, despite its lower quality due to the undersampled nature of the images, enabled us to estimate the relative magnitudes of stars with overlapping apertures.

3.2. Photometric Corrections

We performed all the photometric corrections described in detail in Wang et al. (2011), which included exposure time normalization, zeropoint correction, sigma rescaling, residual flat fielding, time calibration, masking of satellite trails and saturated regions, spike filtering, and magnitude calibration. We will only discuss the details of magnitude and time calibration since the rest of the procedures were identical to our previous work.

We performed the magnitude calibration by matching the mean instrumental magnitudes of 1831 stars with $9.3 \leqslant i \leqslant 12.3$ mag in common between our 2010 and 2008 master frames. Since the mean instrumental magnitudes of each season are referenced to individual images obtained under the best observing conditions (in terms of sky background and number of stars), we would expect them to reflect photometric conditions and therefore have very similar zeropoints. Indeed, we found a zeropoint offset of only 0.018 ± 0.005 mag as shown in Figure 2. We transformed the instrumental magnitudes to the Sloan photometric system by applying the offset of 7.45 ± 0.04 mag previously derived in Section 3.2 of Wang et al. (2011). That offset was based on the comparison of our photometry with the *i* synthetic magnitudes derived by Ofek (2008) using the *Tycho* catalog, which carries an additional systematic uncertainty of 0.02 mag.

Figure 3 shows a time series and a histogram of differential extinction values, based on the photometry procedures described above. We find that extinction due to clouds in the *i* band at Dome A is less than 0.4 mag during 70% of the dark time, and less than 0.1 mag during 40% of the dark time. These values are similar to those previously derived for the 2008 Antarctic winter season (80% and 50%, respectively, from Wang et al. 2011).

The computer associated with the CSTAR#3 telescope has a GPS receiver to maintain time synchronization, and this time was to be distributed to computers controlling the other CSTAR telescopes (including the one used for these observations). However, there was a communication problem between the computers throughout the entire observation period, which led to a drift in the time stamp of the FITS images. Section 4.3 of Zhou et al. (2010a) contains details of the time calibration for

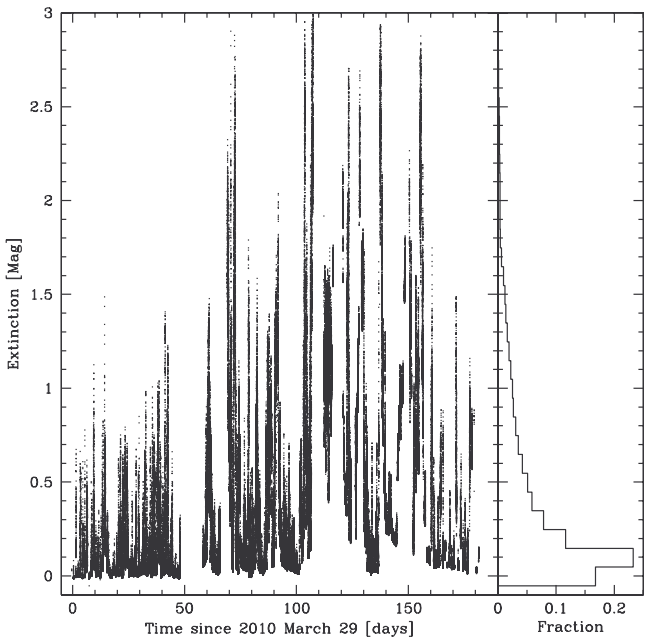

Figure 3. Left panel: time series plots of differential extinction, right panel: distribution of differential extinction.

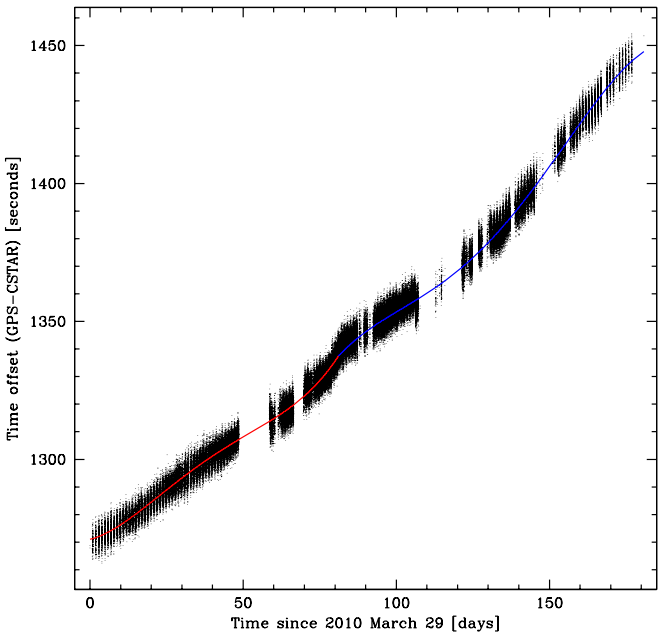

Figure 4. Drift between true local time and computer time, fitted by two fourth-order polynomials.

(A color version of this figure is available in the online journal.)

the 2008 data; we carried out a similar procedure for the 2010 data as explained below.

We performed the time calibration in three steps. First, we identified two bright stars located very close to R.A. = 0h and measured the angle (with respect to the x-axis) of a line extending from the SCP to their positions. We calculated the difference between the measured angle and the one predicted from the time in the FITS headers, and fit a fourth-order polynomial to solve for the time drift. The smallest dispersion was obtained by fitting two different polynomials for the data acquired before and after 2010 June 17. The total clock drift over 6 months amounted to ∼190 s as seen in Figure 4. Next, we used 19 entries in a log (obtained for engineering purposes throughout the season) that listed the time offset between the CSTAR#3 computer and another computer at Dome A that had maintained GPS synchronization. While these data points were not sufficient to solve for the time drift, they served to transform our relative measurements into an absolute reference frame. We obtained an offset of 1337.5 ± 1.6 s. Lastly, we applied a transformation to the heliocentric reference frame.

We later checked the derived time offset by performing a cross-correlation of the light curves of 33 bright, high-amplitude periodic variables (such as eclipsing binaries and RR Lyraes) that we had previously detected in Wang et al. (2011). We used the latest implementation of the Phase Dispersion Minimization algorithm (Stellingwerf 1978, 2011), which can robustly handle large gaps in the time series and combines all light curve "segments" to determine a common period. Using this approach, we found a consistent (but less precise) offset of 1270 ± 245 s.

4. VARIABLE STARS IN THE CSTAR FIELD

While the primary goal of CSTAR observations is to characterize the observing conditions at Dome A, the rapid cadence of image acquisition and the long duration of the winter night make this a relatively unique data set for studying variable stars and searching for extrasolar planets via the transit method. We used several complementary techniques (described below) to identify variables among the selected stars, since no single approach is sensitive to all types of stellar variability. Some of the methods we used are only sensitive to periodic variability. Most of the algorithms we used are available as part of the VARTOOLS light curve analysis program of Hartman et al. (2008).

Having already characterized the observing conditions at the site based on all the "dark time" data, we restricted our variable-star analysis to the images obtained under the best observing conditions, which we defined as a sky background below 100 ADU s^{-1} and an extinction $\leqslant$0.5 mag. These criteria were met by 169,500 frames (the "science-quality" sample), corresponding to about 60.9% of the previously selected set of images. Among the rejected images, 3.7% failed to provide a reliable coordinate transformation with respect to the reference frame.

We initially selected the brightest 20,000 stars in the master frame (corresponding to a depth of $i \sim 15.3$ mag) for time-series aperture photometry. Once the measurements were carried out, we restricted our analysis to 9125 objects with valid measurements in at least 20% of the individual science-quality frames (or in 20% of all possible 3000 s time segments) in order to ensure sufficient synoptic coverage. This restriction implies a maximum declination limit of $-87^\circ 13'$ for objects in the sample, which we will later use when comparing our variable star statistics with previous studies.

We complemented the search for variables with information obtained from the PSF photometry previously carried out on the master frame, which had a 4× finer pixel scale and represented a 24 hr average stellar flux. For each object of interest, we calculated the fraction of contaminating flux contributed by all other stars located closer than a certain distance: the aperture radius (39.″3), the inner edge of the sky annulus (62.″8), and the outer edge of the sky annulus (109.″9). We refer to these three fluxes hereafter as "close," "medium," and "far," respectively.

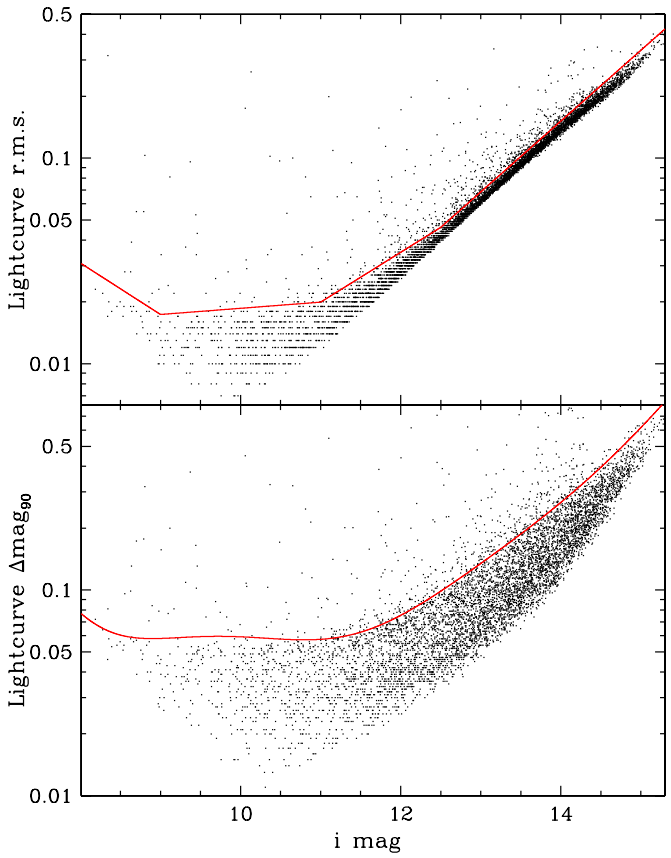

Figure 5. rms (top) and 90 percentile magnitude range (bottom) of the lightcurves of 9125 selected stars with sufficient synoptic coverage (see the text for details).

(A color version of this figure is available in the online journal.)

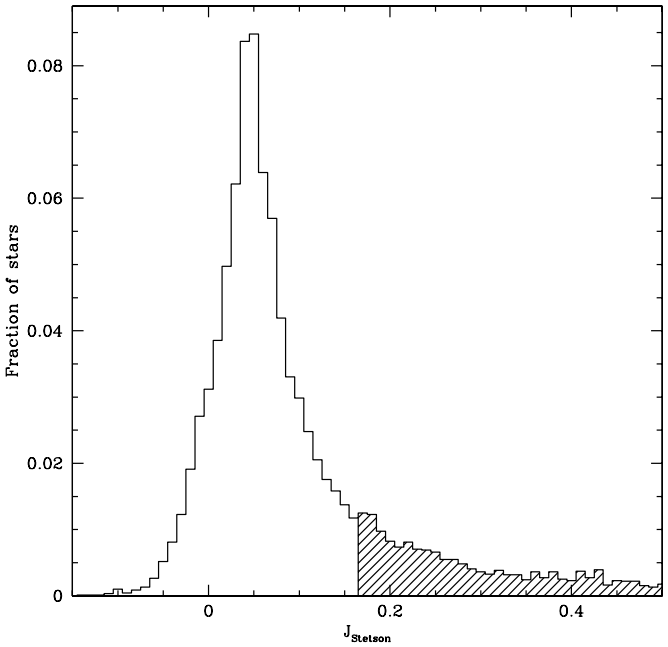

Figure 6. Variability statistic J (Stetson 1996) for 9125 selected stars with sufficient synoptic coverage (see the text for details).

4.1. Search for Variability

The first phase of our search for variable stars was aimed at identifying objects with statistically significant variations in magnitude that did not necessarily display a periodic behavior during our observations—including objects such as Miras, other very long period variables, and irregular variables. We used a combination of three metrics to separate constant from variable stars, as detailed below.

We calculated the rms and the magnitude range spanned by 90% of data points (hereafter Δi_{90}) of the light curves of all stars. We determined upper 2σ envelopes for both quantities as a function of magnitude, shown with red lines in Figure 5. Stars lying above both envelopes were flagged as possible variables for further analysis. The upturn in both envelopes for $i < 9$ mag is probably due to a combination of factors, including the onset of non-linearity in the detector and the dearth of truly constant stars in this magnitude range within our field. The Besançon model of the Galaxy (Robin et al. 2003) predicts that post-main-sequence stars (which are very likely to exhibit variability; see Henry et al. 2000) will outnumber main-sequence objects by a ratio of 7 to 1 at this magnitude.

The lowest light curve rms values (7 mmag) are found at $i \sim 10$ mag, reaching within a factor of five of the expected scatter due to scintillation (Young 1967) for our telescope at Dome A. Given the large number of individual measurements in our photometry, bright ($i < 13.5$ mag) stars lying below both envelopes have statistical uncertainties in their mean magnitudes below 2×10^{-4} mag. As discussed in Section 3.2 and in Wang et al. (2011), the overall uncertainty of the photometry is dominated by the statistical (± 0.04 mag) and systematic (± 0.02 mag) uncertainties of the calibration procedure.

Next, we computed the Welch–Stetson variability index J (Section 2 of Stetson 1996), including the usual rescaling of the reported DAOPHOT magnitude errors (Udalski et al. 1994; Kaluzny et al. 1998). The result of this analysis is shown in Figure 6; as expected for the J statistic, there is a Gaussian distribution of values with a mean value close to zero (corresponding to stars with no significant variability), and a one-sided tail (toward positive values) of candidate variable stars. We determined a mean value of $J = 0.049 \pm 0.038$ by fitting a Gaussian function to all objects with $|J| < 0.3$, and flagged stars with $J \geqslant 0.164$ (equivalent to a $+3\sigma$ selection) for further inspection.

We combined the rms, Δi_{90}, and J criteria listed above to select 44 variable stars. In addition to passing all three variability criteria, the selected objects were also restricted to have contaminating fluxes from nearby companions in the "medium" and "far" apertures below 11.5% and 23% of the total flux, respectively. These limits may have resulted in the rejection of some bona fide aperiodic variables or transient events, but they serve to eliminate false positives from our sample.

4.2. Search for Periodic Variability

The J statistic was designed to be sensitive to statistically significant photometric variability between neighboring data points, and is well suited to detect continuously varying objects such as pulsating stars (Miras, Cepheids, RR Lyrae, δ Scuti, etc.) or contact binaries. It is not particularly sensitive to detached eclipsing binaries (where the variation is restricted to a very small fraction of the phase) or to objects where the variation only becomes statistically significant after phasing many cycles (such as transiting exoplanets or very low amplitude pulsators). Similarly, the other two metrics used in the first phase of the search for variables (light curve rms and Δi_{90}) lack sensitivity to small-scale periodic variations. Therefore, we searched for

Table 3
Variable Stars

ID			R.A.	Decl.	i	Δi_{90}	J	Period		T_0[3]	Class[4]	Note[5]
2010	2008	GSC	(J2000.0)[1]		(mag)			(days)	Src[2]	(days)		
n010320	...	S742000016	12:04:48.75	−87:23:06.0	8.79	0.18	9.68	...	...	...	IR	A
n012443	001707	S74D000321	12:32:42.91	−87:26:22.9	11.10	0.55	9.95	0.338544	LS	785.6824	EC	A
n012506	...	S3Y9000067	11:44:32.67	−87:27:35.9	10.89	0.12	2.07	31.447988	LS	...	MP	
n015318	003125	S3YM000469	10:43:46.63	−87:25:10.1	9.69	0.09	3.32	3.602742	LS	...	MP	
n015705	...	S3YM000358	10:04:32.92	−87:13:44.7	10.97	0.08	0.65	19.081678	LS	...	MP	

Notes. (1) From GSC2.3 except for #n116380 (based on CSTAR master image) (2) LS: Lomb–Scargle method; BLS: box-fitting algorithm. (3) Epoch of primary eclipse or minimum light in JD-2454500. (4) Classes: DS: δ Scuti; EC/ED/ES: eclipsing binary (contact, detached, semi-detached); GD: γ Doradus; IR: irregular; LT: long-term variation; MP: multi-periodic; PR: unclassified periodic; RL: RR Lyrae; TR: transit-like eclipse; (5) A: in ASAS catalog; G: in GCVS.

(This table is available in its entirety in machine-readable and Virtual Observatory (VO) forms in the online journal. A portion is shown here for guidance regarding its form and content.)

periodic variability among the stars that had failed one or more of the previous selection criteria using two of the techniques described in detail in Wang et al. (2011): the Lomb–Scargle method (Lomb 1976; Scargle 1982; hereafter LS) and the "box fitting algorithm" of Kovács et al. (2002; hereafter BLS).

Given the design of the CSTAR system, stars describe daily circular tracks through the CCD. This can lead to spurious detections of periodicity due to small residual flat-field variations. Fortunately, these false positives are easily identified and discarded because the variations occur at frequencies close (0.5%–3%) to 1 cycle per sidereal day and their (sub-)harmonics. We considered an object to have significant periodic variability if the period determined by VARTOOLS (based on either the LS or the BLS technique) had a signal-to-noise ratio > 30 and lied outside of the excluded frequencies. We imposed a minimal restriction on contaminating flux for this search, removing 2% of objects where the contaminating flux from other stars in the "close" aperture exceeded 40% of the total. The search for periodic variables can tolerate substantially larger contamination from neighbors for several reasons: very close neighbors (within the instrumental PSF or the measurement aperture) can only decrease the amplitude of the variation but cannot result in a false positive, and future observations can be used to identify which of the confused stars is the actual variable; stars outside the measurement aperture but within the outer sky annulus may produce noisier measurements but the long span of our observations still yields high-quality binned light curves that satisfy the requirement on the signal-to-noise ratio of the period determination; any companions that somehow induce a spurious periodic variation will do so at frequencies of 1 cycle day^{-1}, or one of its harmonics, and those have already been removed from consideration.

We detected an additional 136 variables using the LS technique and a further 8 variables using the BLS technique. These algorithms were also applied to the variables previously selected in Section 4.1 and 16 of those objects were found to exhibit a significant periodicity. The initial periods were refined using the Period04 program (Lenz & Breger 2005) and the Phase Dispersion Minimization algorithm (Stellingwerf 1978, 2011).

Approximately two-thirds of the periodic variables exhibit a highly regular variation both in terms of period and amplitude (e.g., eclipsing binaries, normal RR Lyraes), a few have a long-term modulation in amplitude (e.g., Blazhko RR Lyraes), and about one-third show variations at multiple frequencies. In the latter two cases, we based our analysis in the most significant period.

4.3. Properties of Variable Stars

Table 3 lists the properties of all detected variables. Column 1 has the 2010 CSTAR ID (a letter "n" is added at the beginning to avoid confusion with 2008 CSTAR IDs from our previous work); Column 2 lists the 2008 CSTAR ID from Wang et al. (2011), if applicable; Column 3 presents the ID from the Guide Star Catalog, version 2.3.2 (GSC2.3), when available; Columns 4 and 5 give the right ascension and declination; Column 6 contains the mean i-band magnitude; Column 7 lists the 90% range of the i-band light curve; Column 8 has the J value; Column 9 lists the most significant period (when applicable); Column 10 specifies the technique used to find the period; Column 11 gives the first time of minimum light contained in our observations (listed only for the periodic variables); Column 12 contains a tentative classification of the variable type, when possible; Column 13 has additional information, including previous identification of the variables by the All-Sky Automated Survey (ASAS; Pojmanski 2005) or inclusion in the General Catalog of Variable Stars (GCVS; Samus et al. 2009). Representative light curves of periodic variables are shown in Figure 7, while two-season light curves of selected long-term variables are plotted in Figure 8. Detailed finding charts including light curve plots for all variables are available through the Chinese Virtual Observatory.[14] All light curve data are also available through this site.

We detected a total of 188 variables in the 2010 CSTAR data, consisting of 67 new objects and 121 stars in common with Wang et al. (2011). We did not recover 36 objects classified as variables in our previous paper for the following reasons: 10 did not have enough data points, 7 were blended, and 19 did not meet the selection criteria adopted in this paper. The new variables detected in this study relative to our previous work were made possible by the deeper magnitude limit and slightly larger field of view ($\delta < -87^\circ 13'$) of the 2010 observations, which were respectively due to better sky subtraction and improved alignment of the center of the field with the SCP.

Thanks to the greater depth and synoptic coverage of our observations, we obtained a $\sim 4\times$ increase in the number of variables with $\delta < -87^\circ 13'$ relative to previous surveys. For example, our observations reach $i \sim 15.3$ mag while the previous study of this area of the sky by ASAS reached a limiting magnitude of $V \sim 14.5$ mag (equivalent to $i \sim 13$–14.5 mag depending on spectral type). We recovered 35

[14] http://casdc.china-vo.org/data/cstar

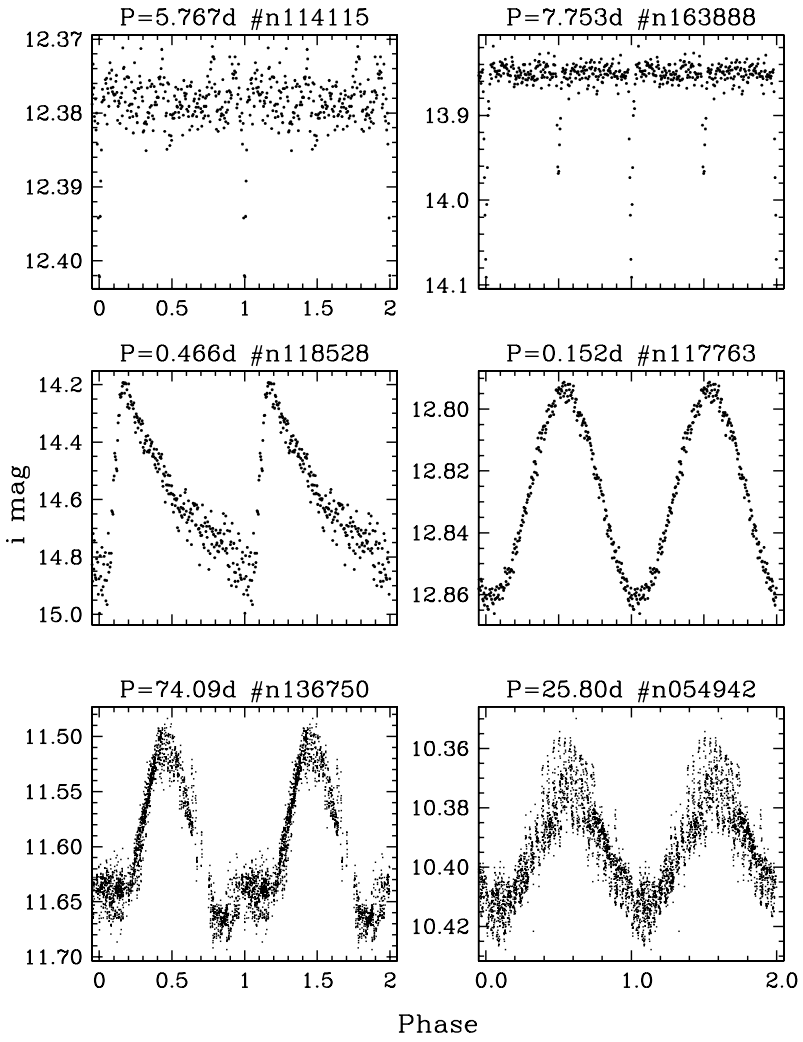

Figure 7. Phased light curves of six newly detected periodic variable stars. The periods and 2010 CSTAR IDs are given above each panel. Top row: transiting exoplanet candidate and detached eclipsing binary; middle row: RR Lyrae and δ Scuti; bottom row: multi-periodic variables phased at the most significant period.

of the 46 previously known variables in our field; 5 were saturated, 3 were strongly blended, and 3 did not meet our minimum requirement for synoptic coverage.

Our observations found significant variability or periodicity for 2.1% of the stars in the sample. This variable star fraction is in good agreement with the expectation for a survey like ours with a photometric precision limit of ~0.02 mag (see Figure 9 of Tonry et al. 2005). Among the 44 variables selected by the analysis of Section 4.1, which did not discriminate by type of variability, 11% are strictly periodic (eclipsing binaries, RR Lyraes, etc.), an additional 25% exhibit multi-periodic behavior, and the remaining 64% have no significant periodicity.

Table 4 lists statistics for the different types of objects we detected based on both searches (Sections 4.1 and 4.2). The variable types are consistent with expectations for a red-sensitive survey directed toward a halo field. For example, nearly half of all variables exhibit low-amplitude/multi-periodic or long-term/irregular pulsations typical of red giant branch or asymptotic giant branch stars. Ninety percent of the variables of these types present in our sample have $i < 12$ mag, and according to the Besançon model of the Galaxy (Robin et al. 2003), post-main-sequence stars dominate the stellar population of our field in that magnitude range. The regular pulsators that we have been able to classify based on light curve shape or period are also post-main-sequence or Population II objects, such as RR Lyrae or δ Scuti stars. In contrast, the eclipsing binaries and unclassified periodic variables have a broader distribution in magnitude, as expected for a mix of evolved and main-sequence objects.

Table 4
Distribution of Variable Star Types

Variable Type	*N*	%
Multi-periodic	57	30.3
Unclassified periodic	47	25.0
Eclipsing binaries	35	18.6
Irregular/long-term	28	14.9
δ Sct	8	4.3
RR Lyr	7	3.7
γ Dor	3	1.6
Transit-like	3	1.6

We combined the two years of CSTAR photometry (from the 2008 and 2010 Antarctic winters) to search for changes in the observed properties of the variables. The very fast periodic variable #n090586 exhibited the same three significant frequencies first seen in the 2008 observations (see Figure 17

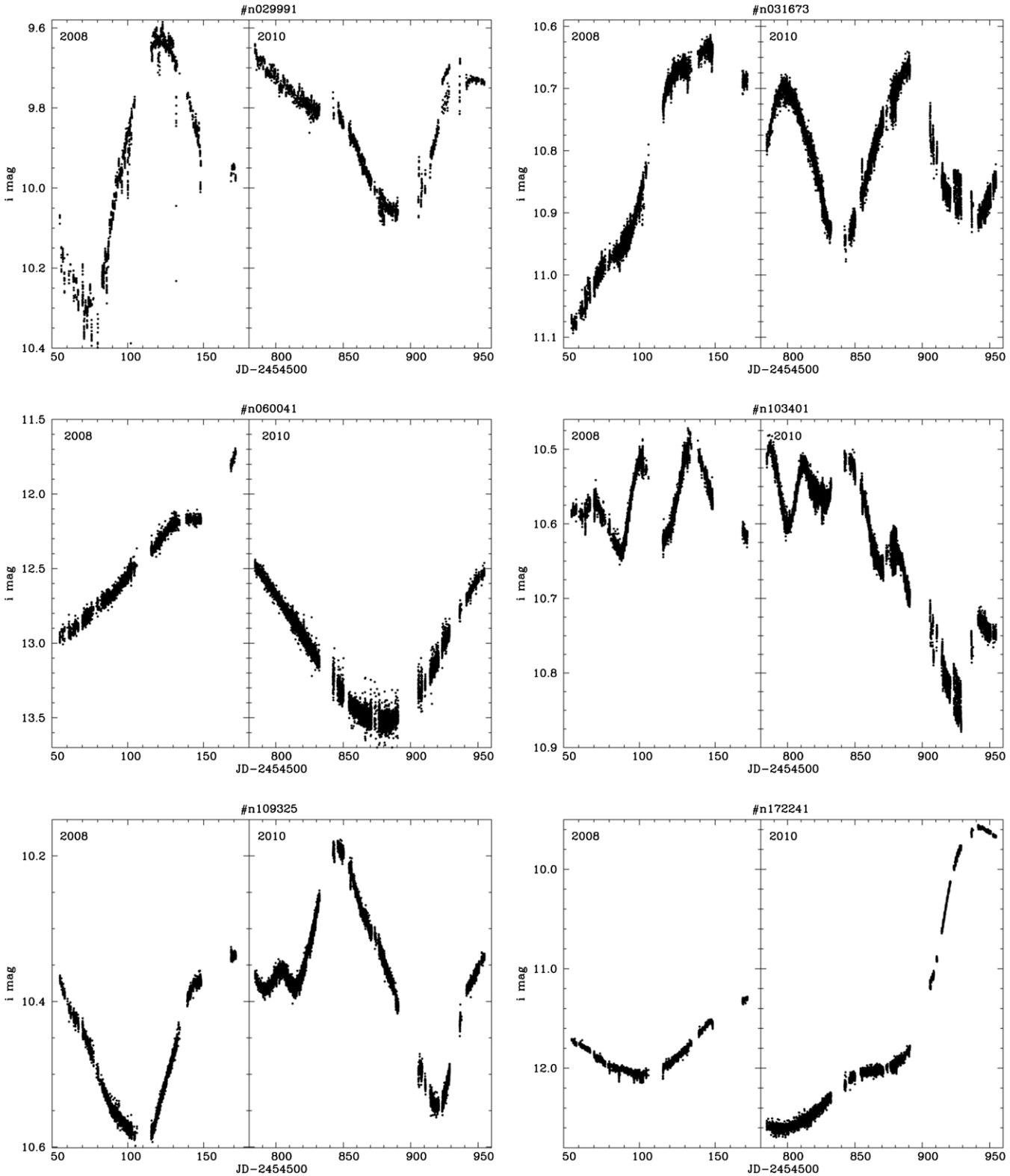

Figure 8. Two-year light curves (left: 2008; right: 2010) for variables with long-term trends.

of Wang et al. 2011), but the amplitude of each component exhibited significant temporal variations relative to that season (at the $-3.8, 7.8$, and 11.4σ level, respectively). A comparison of the first and second halves of the 2010 data (Figure 9) also shows a significant (-3.9σ) variation for one of the frequencies. We plan to do further research on this object using a fast-pulsating stellar model.

The 2010 light curve of CSTAR#n057725 ($P = 43.2$ days), originally discovered by the ASAS project (Pojmanski 2005) and classified as a fundamental-mode δ Cephei variable, showed a dramatic change relative to 2008, as seen in Figure 10. The Cepheid-like variability seen in the 2008 data (top-left panel), which already showed indications of a change in amplitude, decreased even further and developed a secondary peak in the

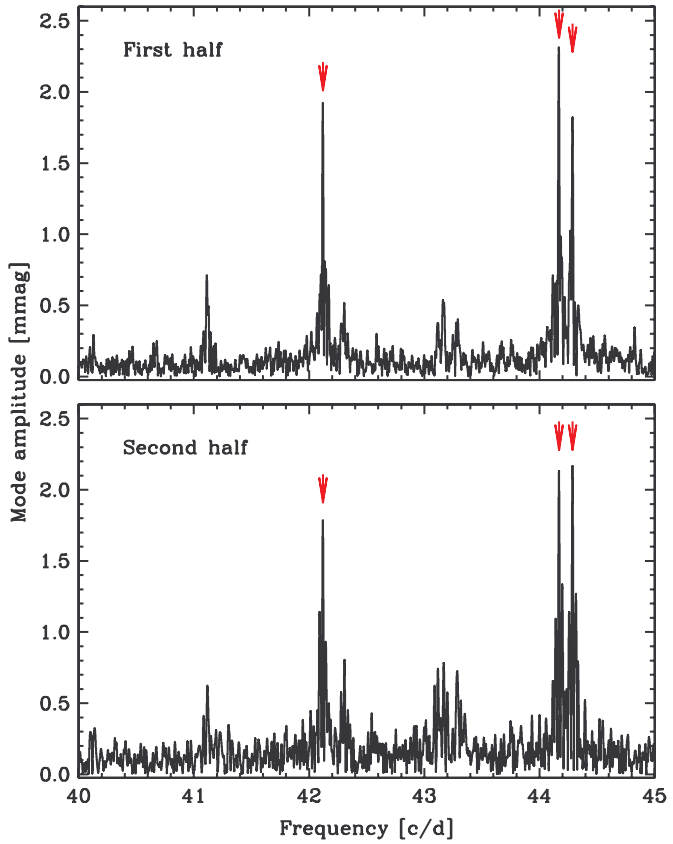

Figure 9. Fourier spectrum of CSTAR #n090586 derived using the Period04 program, based on data obtained during the first (top) and second (bottom) half of the 2010 season. Three significant peaks (at f_i = 44.288, 44.169, and 42.121 cycles day^{-1}) are detected with varying amplitudes, which exhibit significant changes (4–11σ) relative to the 2008 season. See the text for details.
(A color version of this figure is available in the online journal.)

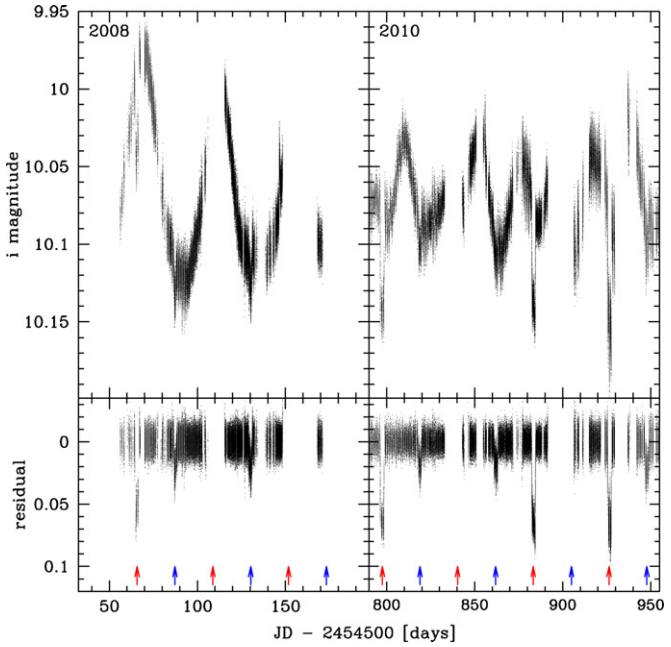

Figure 10. Light curve of CSTAR#n057725, showing the slow reduction in Cepheid-like pulsation amplitude during the 2008 season has been replaced by a more complex variability in 2010. Eclipse-like events seem to be present at two distinct phases indicated with red and blue arrows, respectively.
(A color version of this figure is available in the online journal.)

2010 data (top-right panel). Furthermore, eclipse-like events can now be seen at two distinct phases of the pulsation (bottom panels) separated by half of the period with depths of ∼0.07 and ∼0.03 mag. The *V*-band ASAS light curve, spanning more than a decade, also shows secular variations in pulsation amplitude. The ASAS classification of this object is very unlikely; at i = 10.1 mag, a 43 day Cepheid would lie ∼17 kpc away and nearly 8 kpc above the Galactic plane, an extremely improbable location for an ∼11 $M_\odot$ star. It is more likely that this object consists of a Population II pulsator, such as an RV Tauri or the Galactic equivalent of an Optical Gravitational Lensing Experiment small-amplitude variable red giant (Soszynski et al. 2004) in a binary system. We plan to undertake additional observations to investigate the nature of this system.

5. CONCLUSIONS AND SUMMARY

We have presented the analysis of high-cadence synoptic observations of 23 deg^2 centered on the south celestial pole, conducted with the CSTAR#3 telescope at Dome A during 183 days of the 2010 Antarctic winter season. Eighty-six percent of all frames obtained at a sun elevation angle below 0° yielded useful data. We measured a median sky background of 19.8 mag arcsec^{-2} over all moon phases and determined that the extinction is below 0.1 mag for 40% of the time (0.4 mag for 70% of the time). All these values are consistent with the site statistics derived from the 2008 season, and reinforce the promise of the Antarctic Plateau for future astronomical work.

We carried out time-series aperture photometry of 9125 stars with i < 15.3 mag. We detected 188 variable stars, including 67 new objects not included in our previous work thanks to a slightly larger field of view and a deeper magnitude limit. This represents a ∼4× increase in the number of variable stars relative to previous surveys of the same region of the sky. We plan follow-up multi-wavelength photometry and high-resolution spectroscopy in the near future of the most interesting variables, such as detached eclipsing binaries and the candidate transiting exoplanets.

Given the coarse pixel scale of our images and our use of aperture photometry, the search for (non-periodic) variable stars was limited to objects with low levels of crowding. This could be mitigated by the use of difference imaging techniques in future analyses. The apparent circular motion of stars in the field of view, due to the fixed nature of the telescope and camera, prevented the detection of periodic variability at frequencies close to one sidereal day (and its harmonics) despite the absence of a day/night cycle and the long duration of the observations. Future surveys conducted from Antarctica would greatly benefit from instruments with improved angular resolution, a finer pixel scale, and the ability to track. The recently deployed AST3 telescopes (Cui et al. 2008) meet all these criteria and should greatly expand our synoptic capabilities in the polar regions.

L.W. acknowledges support by the BaiRen program of the Chinese Academy of Sciences (034031001); the National Natural Science Foundation of China under the Distinguished Young Scholar grant 10825313 and grants 11073005 and 11303041; the Ministry of Science and Technology National Basic Science Program (Project 973) under grant number 2012CB821804; the Excellent Doctoral Dissertation of Beijing Normal University Engagement Fund; and a Young Researcher Grant of the National Astronomical Observatories, Chinese Academy of Sciences.

L.M. and L.W. acknowledge support by the Department of Physics and Astronomy at Texas A&M University through faculty startup funds and the Mitchell–Heep–Munnerlyn Endowed Career Enhancement Professorship in Physics or Astronomy.

This work was supported by the Chinese PANDA International Polar Year project, NSFC-CAS joint key program through grant number 10778706, CAS main direction program through grant number KJCX2-YW-T08, and by the Chinese Polar Environment Comprehensive Investigation and Assessment Programs (CHINARE). The authors deeply appreciate the great efforts made by the 24–28th Dome A expedition teams who provided invaluable assistance to the astronomers that set up and maintained the CSTAR telescope and the PLATO system. PLATO was supported by the Australian Research Council and the Australian Antarctic Division. Iridium communications were provided by the US National Science Foundation and the US Antarctic Program.

Facility: Dome A: CSTAR.

REFERENCES

Ashley, M. C. B., Allen, G., Bonner, C. S., et al. 2010, HiA, 15, 627
Burton, M. G. 2010, A&ARv, 18, 417
Charbonneau, D., Brown, T. M., Latham, D. W., & Mayor, M. 2000, ApJL, 529, L45
Cui, X., Yuan, X., & Gong, X. 2008, Proc. SPIE, 7012, 70122D
Hartman, J. D., Gaudi, B. S., Holman, M. J., et al. 2008, ApJ, 675, 1254
Hengst, S., Allen, G. R., Ashley, M. C. B., et al. 2008, Proc. SPIE, 7012, 70124E
Henry, G. W., Fekel, F. C., Henry, S. M., & Hall, D. S. 2000, ApJS, 130, 201
Howell, S. B. 2012, PASP, 124, 263
Kaluzny, J., Stanek, K. Z., Krockenberger, M., et al. 1998, AJ, 115, 1016
Kenyon, S. L., Lawrence, J. S., Ashley, M. C. B., et al. 2006, PASP, 118, 924
Kovács, G., Zucker, S., & Mazeh, T. 2002, A&A, 391, 369
Lawrence, J. S., Allen, G. R., Ashley, M. C. B., et al. 2008, Proc. SPIE, 7012, 701227
Lawrence, J. S., Ashley, M. C. B., Burton, M. G., et al. 2006, Proc. SPIE, 6267, 62671L
Lawrence, J. S., Ashley, M. C. B., Hengst, S., et al. 2009, RScI, 80, 064501
Lenz, P., & Breger, M. 2005, CoAst, 146, 53
Lomb, N. R. 1976, Ap&SS, 39, 447
Luong-van, D. M., Ashley, M. C. B., Cui, X., et al. 2010, Proc. SPIE, 7733, 77331T
Mosser, B., & Aristidi, E. 2007, PASP, 119, 127
Nugent, P. E., Sullivan, M., Cenko, S. B., et al. 2011, Natur, 480, 344
Ofek, E. O. 2008, PASP, 120, 1128
Pojmanski, G. 2005, VizieR On-line Data Catalog (originally published in Pojmanski, G. 2000, AcA, 50, 177)
Robin, A. C., Reylé, C., Derrière, S., & Picaud, S. 2003, A&A, 409, 523
Samus, N. N., Durlevich, O. V., Kazarovets, R. V., et al. 2009, yCat, 10, 2025
Saunders, W., Lawrence, J. S., Storey, J. W. V., et al. 2009, PASP, 121, 976
Saunders, W., Lawrence, J. S., Storey, J. W. V., et al. 2010, in EAS Publ. Ser. 40, 3rd ARENA Conference: An Astronomical Observatory at CONCORDIA (Dome C, Antarctica), ed. L. Spinoglio & N. Epchtein (Cambridge: Cambridge Univ. Press), 89
Scargle, J. D. 1982, ApJ, 263, 835
Schlafly, E. F., & Finkbeiner, D. P. 2011, ApJ, 737, 103
Soszynski, I., Udalski, A., Kubiak, M., et al. 2004, AcA, 54, 129
Stellingwerf, R. F. 1978, ApJ, 224, 953
Stellingwerf, R. F. 2011, in RR Lyrae Stars, Metal-Poor Stars, and the Galaxy, ed. A. McWilliam (Pasadena, CA: The Observatories of the Carnegie Institution of Washington), 47
Stetson, P. B. 1987, PASP, 99, 191
Stetson, P. B. 1996, PASP, 108, 851
Storey, J. W. V. 2005, Antarct. Sci., 17, 555
Storey, J. W. V. 2007, ChA&A, 31, 98
Storey, J. W. V. 2009, Assoc. Asia Pac. Phys. Soc. Bull., 19, 1
Tonry, J. L., Howell, S. B., Everett, M. E., et al. 2005, PASP, 117, 281
Udalski, A., Szymanski, M., Stanek, K. Z., et al. 1994, AcA, 44, 165
Wang, L., Macri, L. M., Krisciunas, K., et al. 2011, AJ, 142, 155
Yang, H., Allen, G., Ashley, M. C. B., et al. 2009, PASP, 121, 174
Young, A. T. 1967, AJ, 72, 747
Yuan, X., Cui, X., Liu, G., et al. 2008, Proc. SPIE, 7012, 70124G
Zhou, X., Fan, Z., Jiang, Z., et al. 2010a, PASP, 122, 347
Zhou, X., Wu, Z., Jiang, Z., et al. 2010b, RA&A, 10, 279
Zou, H., Zhou, X., Jiang, Z., et al. 2010, AJ, 140, 602